Supplementary Material - Small molecule ensembles reshape amyloid aggregation landscapes

Radhika V. Nair[1], Bich Ngoc Tran[2], Atul N. Parikh[1], and Matthew R. Foreman[*1,3]

[1]Institute for Digital Molecular Analytics and Science, Nanyang Technological University, 59 Nanyang Drive, Singapore 636921, Singapore

[2]NTU Institute of Structural Biology (NISB), Nanyang Technological University, Experimental Medicine Building, 59 Nanyang Drive, Singapore 636921

[3]School of Electrical and Electronic Engineering, Nanyang Technological University, 50 Nanyang Avenue, Singapore 639798

*Corresponding author: matthew.foreman@ntu.edu.sg

1 Amyloid beta growth - ThT fluorescence assay and DLS measurements

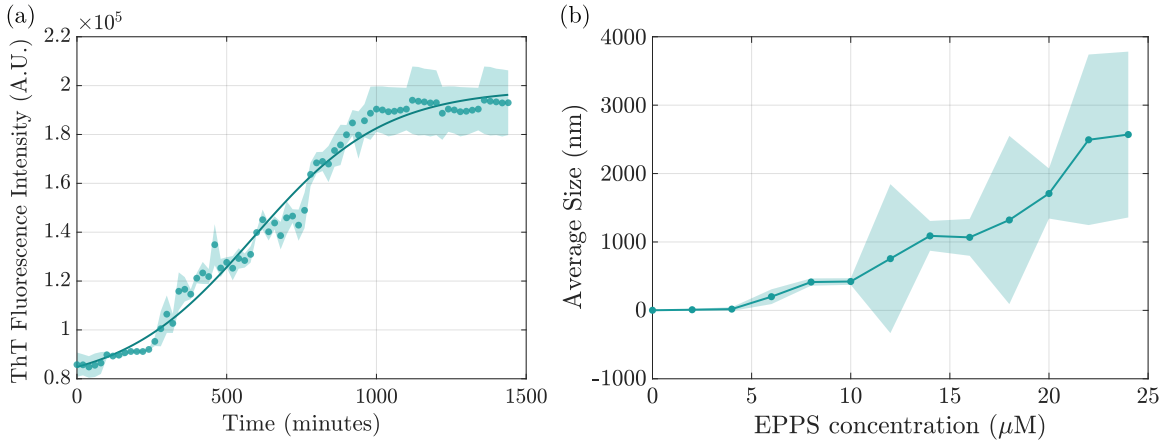

Figure S1: (a) ThT fluorescence versus incubation time showing amyloid beta growth kinetics. The apparent rate constant (k), lag time (t_{lag}), and half-time ($t_{1/2}$) are extracted from the sigmoidal fit as 0.0046 min^{-1}, 587 min, and 150 min, respectively. (b) Dynamic light scattering (DLS) data showing the change in particle size during incubation, reflecting aggregation behavior over time. The solid line in (a) indicates the sigmoidal fit, and the shaded bands in both panels represent the standard deviation from three independent replicates.

2 Steady state ThT data during EPPS treatment

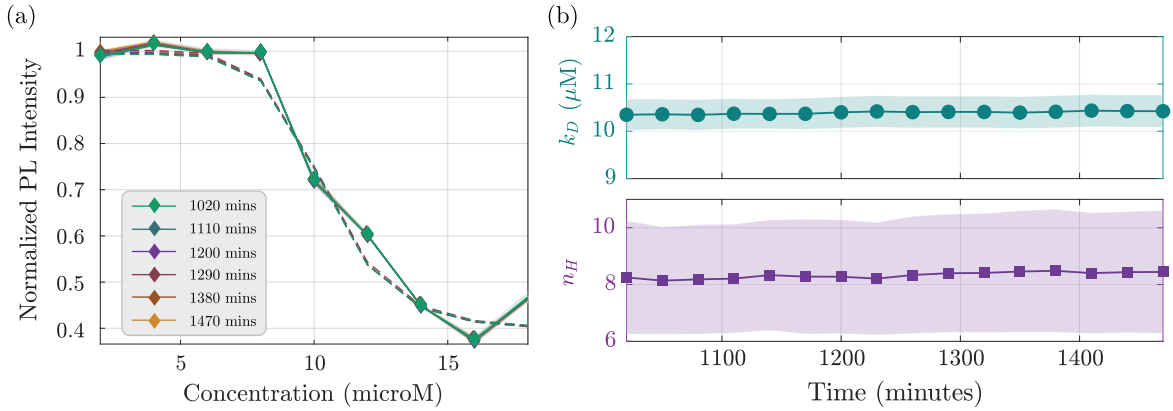

Figure S2: (a) ThT intensity as a function of EPPS concentration at different incubation times during the steady phase (900-1500 minutes, shown as solid curves of different colors). (b) Time-dependent plots of k_D and n_H during the steady state obtained from sigmoidal fit (dashed line). The shaded band in (a) and (b) indicates the standard deviation obtained from 3 independent replicates.

3 Binding isotherm

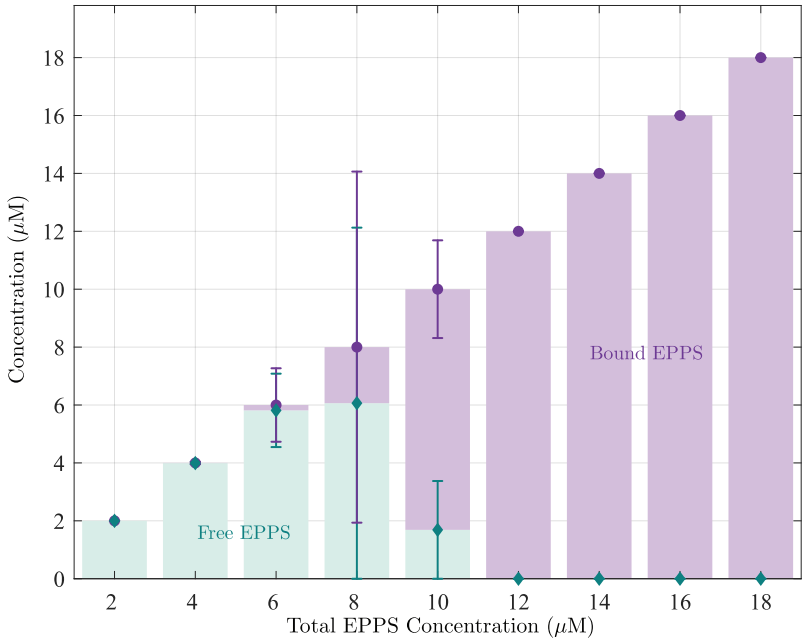

Figure S3: Free and bound EPPS concentrations as a function of total EPPS concentration, derived from Hill fitting of ThT steady-state kinetic data. Error bars represent the standard deviation of calculated free and bound EPPS concentrations from three independent replicates.

4 FTIR measurements

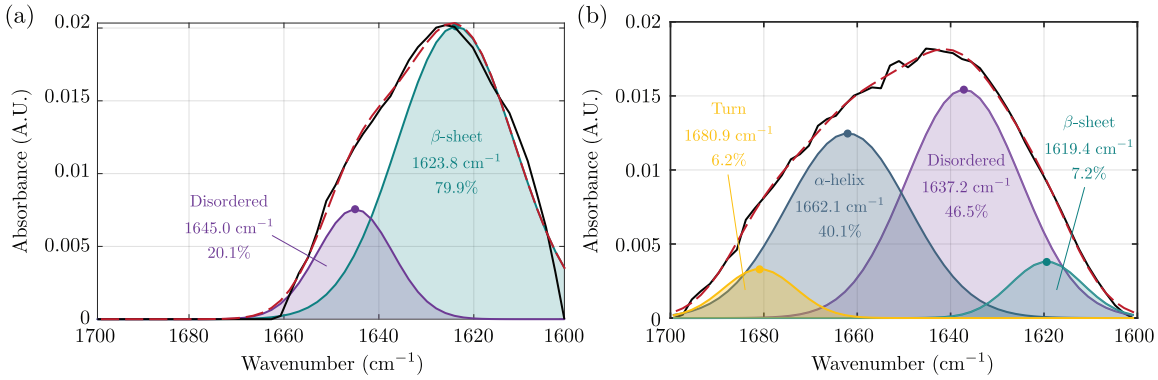

Figure S4: (a) FTIR spectra of amide I region of fully grown amyloid beta fibrils. Deconvolution using pseudo-Voigt fit shows β-sheet as the major component with peak area of ∼80% along with the disordered peak with peak area of ∼20%. (b) FTIR spectra of the amide I region of Aβ after 4 hours of treatment with 10 μM EPPS. Deconvolution using a pseudo-Voigt fit reveals a marked reduction in β-sheet content, accompanied by the emergence of new secondary structural components, consistent with EPPS-induced disaggregation of Aβ fibrils.

5 TEM - EPPS treated Aβ- Longer incubation

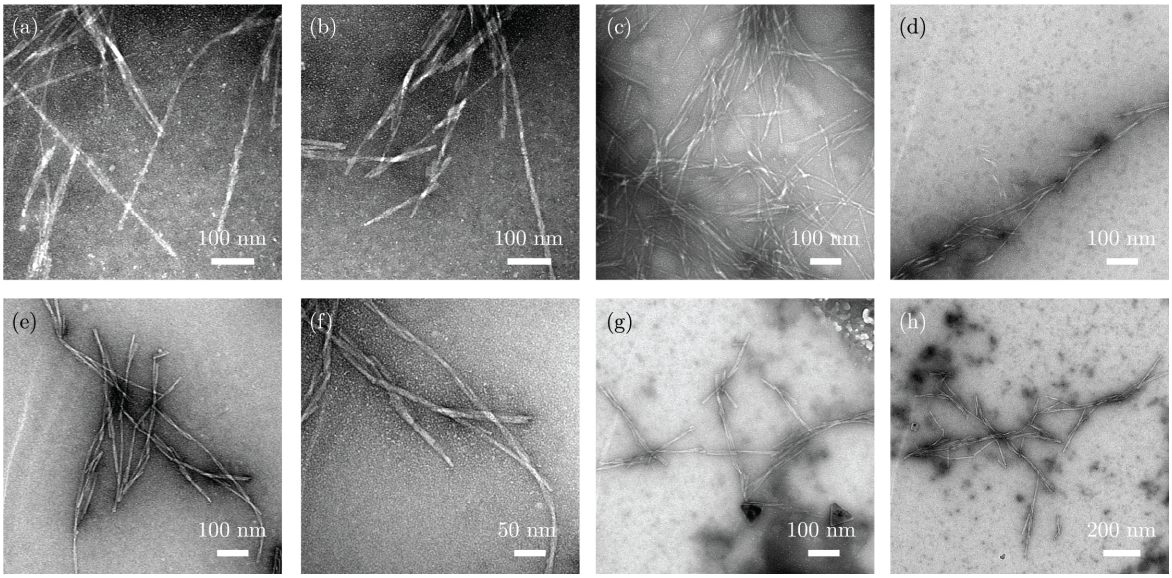

Figure S5: Negative-stain TEM images of Aβ_{42} fibrils under different EPPS concentrations. (a) and (b) 30 μM EPPS treated sample incubated for 4 days. (c) and (d) 30 μM EPPS treated sample incubated for 6 days. (e) and (f) 40 μM EPPS treated sample incubated for 4 days. (g) and (h) 40 μM EPPS treated sample incubated for 6 days

6 Estimated Calculation of EPPS Monomers in Clusters from DLS Measurements

To estimate the percentage of free monomers and clustered species from DLS intensity data, we applied scattering theory principles to convert intensity distributions into approximate number distributions. For clusters larger than 60 nm, we used Mie theory, which accounts for complex size-dependent scattering effects. According to Mie theory, the scattering efficiency Q_{sca} is calculated using the scattering coefficients a_n and b_n as follows [1]

$$Q_{\text{sca}} = \frac{2}{x^2} \sum_{n=1}^{\infty} (2n+1) \left(|a_n|^2 + |b_n|^2 \right),$$

where the size parameter $x = \frac{2\pi r}{\lambda}$, r is the particle radius and λ is the wavelength in the host medium. The coefficients a_n and b_n are given by:

$$a_n = \frac{m\psi_n(mx)\psi_n'(x) - \psi_n(x)\psi_n'(mx)}{m\psi_n(mx)\xi_n'(x) - \xi_n(x)\psi_n'(mx)},$$

$$b_n = \frac{\psi_n(mx)\psi_n'(x) - m\psi_n(x)\psi_n'(mx)}{\psi_n(mx)\xi_n'(x) - m\xi_n(x)\psi_n'(mx)},$$

where $m = \frac{n_{\text{particle}}}{n_{\text{medium}}}$ is the relative refractive index, ψ_n and ξ_n are the Riccati-Bessel functions, and primes denote derivatives with respect to the argument. These coefficients are calculated numerically. The scattered intensity is proportional to the product of the number of particles N, the scattering

efficiency $Q_{\text{sca}}(d)$, and the geometric cross-section ($\propto d^2$), expressed as

$$I(d) \propto N Q_{\text{sca}}(d) d^2$$

where $d = 2r$ is the particle diameter Rearranging this relation allowed us to estimate the raw number distribution from the DLS data as:

$$N_{\text{DLS}}(d) \propto \frac{I(d)}{Q_{\text{sca}}(d) d^2}.$$

To convert this to an absolute number distribution, we calibrated the data using DLS measurements of 500 nm latex beads of known concentration, where the total number N_{latex} was used to calculate a scaling factor:

$$\text{scaling factor} = \frac{N_{\text{latex}}}{\sum_d N_{\text{DLS}}(d)}.$$

The final calibrated number distribution for clusters larger than 60 nm is then:

$$N(d) = \text{scaling factor} N_{\text{DLS}}(d).$$

For clusters smaller than 60 nm, we assumed the Rayleigh scattering regime ($d \ll \lambda$), where intensity per particle follows the [1]:

$$I_{\text{monomer}} \propto d^6,$$

which can be written as $I_{\text{monomer}} = C d^6$ where C is a proportionality constant. Using DLS data from a 1 nM concentration solution of EPPS as the reference monomer data, we calculated the scaling factor for the smaller clusters. The known monomer concentration is:

$$N_{\text{ref}} = c_{\text{ref}} V_{\text{ref}} N_{\text{A}},$$

where N_{A} is Avogadro's number . Using the peak intensity I_{peak} from the reference DLS data, we obtained the scaling factor C by:

$$C = \frac{I_{\text{peak}}}{N_{\text{ref}} d^6}.$$

This allowed us to calculate the expected number of monomers N_{exp} in the sample as:

$$N_{\text{exp}} = \frac{I_{\text{peak}}}{C d^6}.$$

Through this combined approach, using Mie theory for larger clusters calibrated with latex beads and Rayleigh approximation for smaller clusters calibrated with monomer EPPS data, we translated intensity data into an approximate number distribution of free monomers versus clustered species. A monomer hydrodynamic diameter of 1 nm was assumed; all particles with apparent sizes greater than 1 nm were considered as monomers incorporated within clusters. This provided insights into the fraction of EPPS molecules in monomeric and aggregated states as a function of concentration.

7 Effect of ionic strength on EPPS dynamic clustering

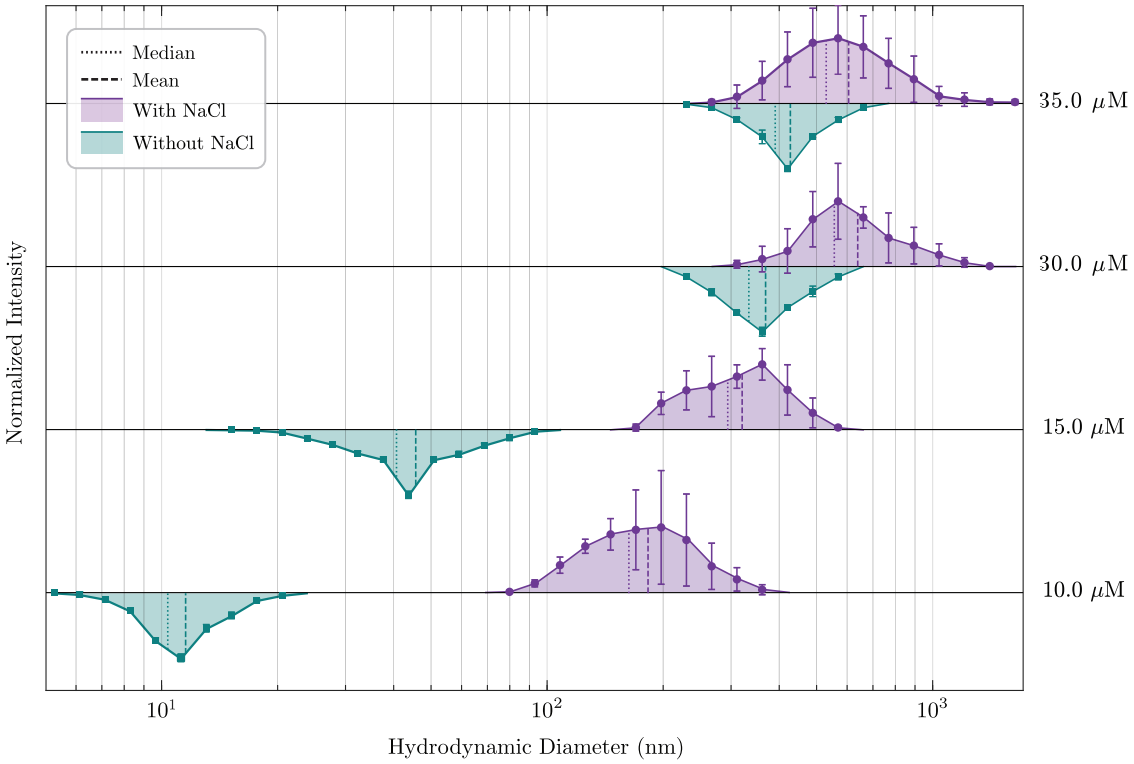

Figure S6: DLS analysis of EPPS dynamic clustering under varying ionic strength via 200 mM NaCl addition. A comparison between the EPPS size distribution with and without NaCl is shown. Addition of NaCl clearly shows an increase in the average cluster size formed. Error bars represent standard deviation from three independent measurements. Dashed lines and dotted lines represent the mean values and median values, respectively. Concentration of EPPS (10-35 μM) is shown on the right margin of the panel.

8 Effect of HEPES treatment on amyloid beta disaggregation

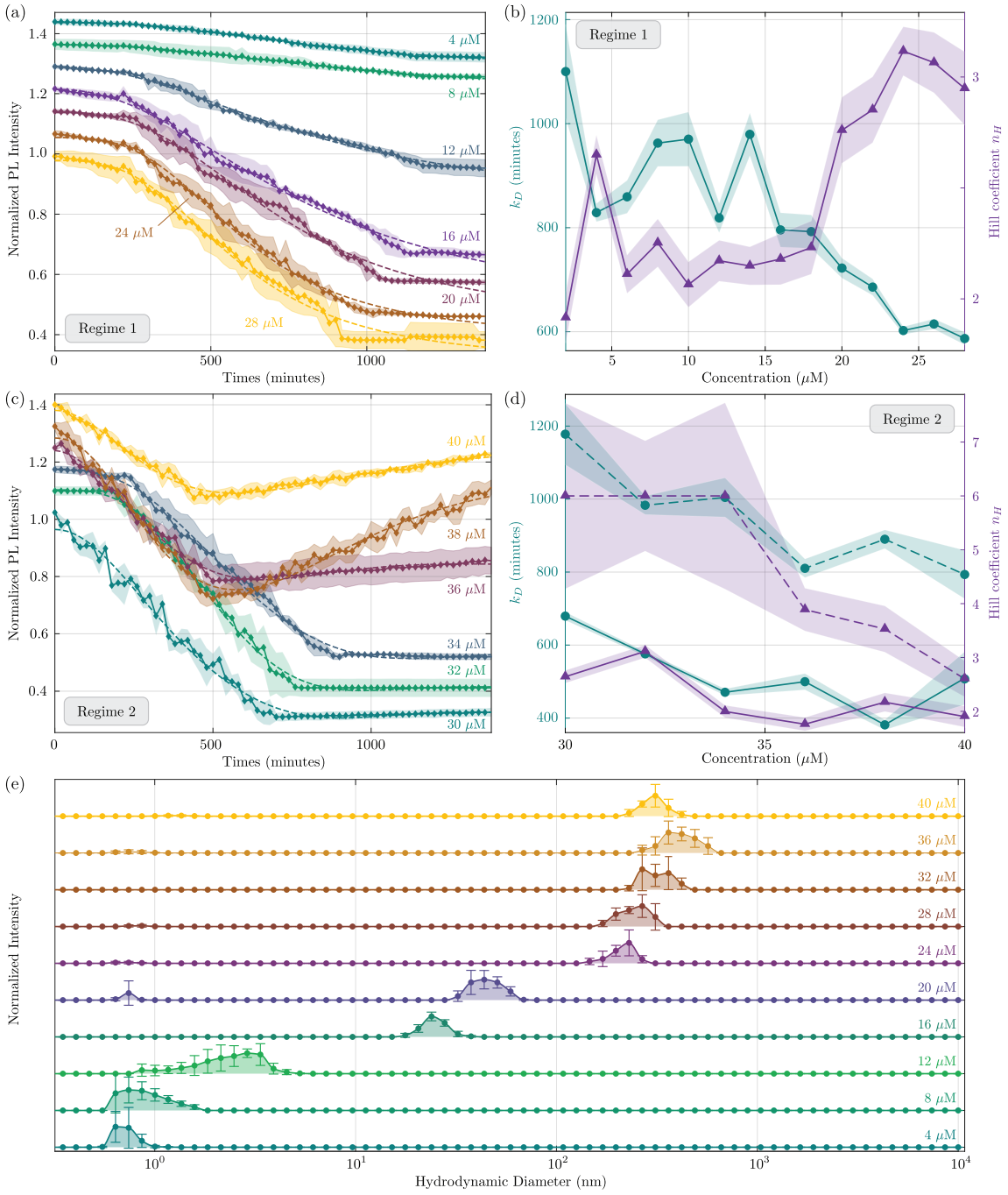

Figure S7: HEPES treatment effects on Aβ aggregation and clustering. (a) ThT PL intensity profiles for Regime 1, (b) ThT PL intensity profiles for Regime 2, (c) Regime 1: k_D and n_H values extracted from Hill fit, (d) Regime 2: k_D and n_H values extracted from double Hill fit, (e) DLS plots showing dynamic clustering of HEPES at various concentrations.

9 TEM images of EPPS-treated PEG crowded Aβ

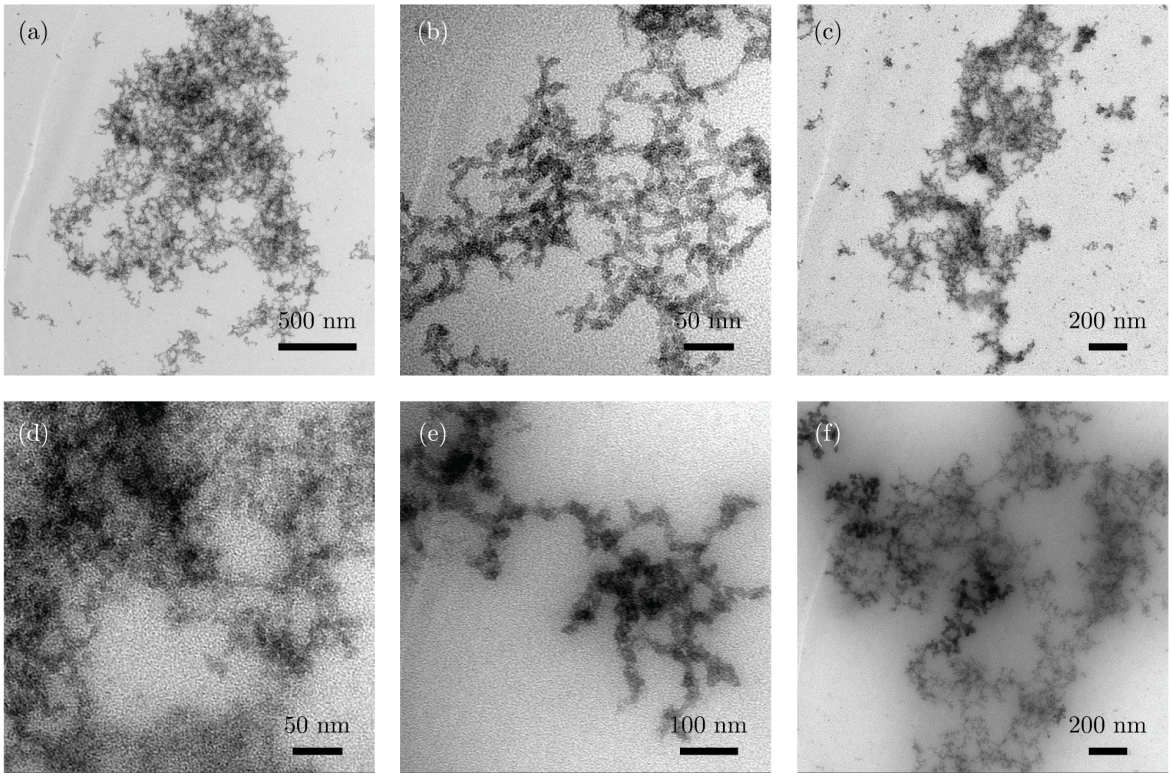

Figure S8: Negative-stain TEM images of PEG crowded Aβ_{42} fibrils treated with various concentrations of EPPS for 24 hours. (a) and (b) 10 μM EPPS treated sample. (c) and (d) 20 μM EPPS treated sample. (e) and (f) 30 μM EPPS treated sample.

10 DLS Analysis of Amyloid Crowding Induced by PEG2000

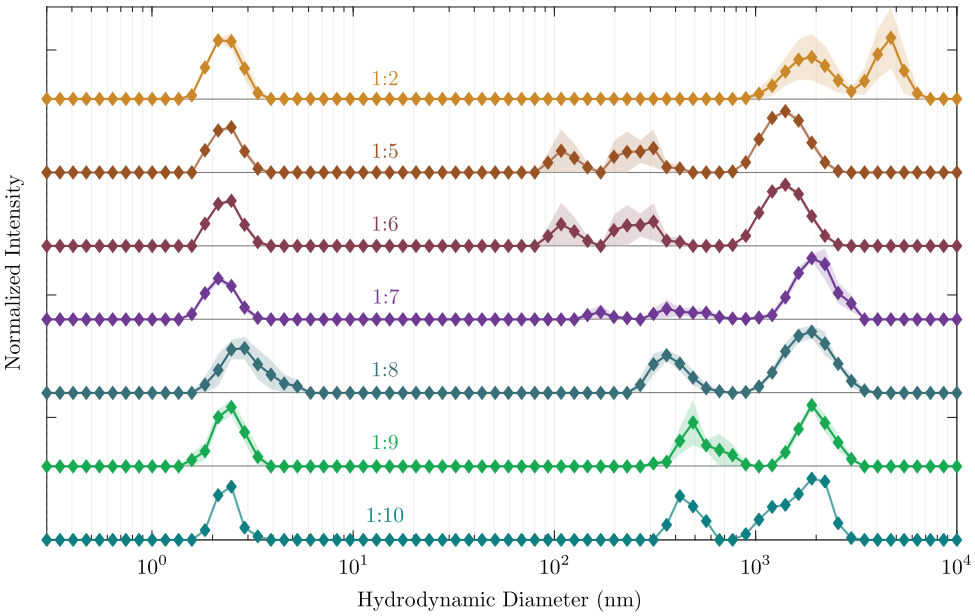

Figure S9: Dynamic light scattering (DLS) intensity versus particle size for amyloid β (Aβ) in the presence of PEG2000 at various crowding ratios. Shaded bands represent the standard deviation from three replicate measurements. The DLS data show large variations in size distribution, as evident from the standard deviation, indicating that PEG2000 crowding results in heterogeneous clusters within the sample.

11 ThT fluorescence of EPPS treated PEG-crowded fibrils

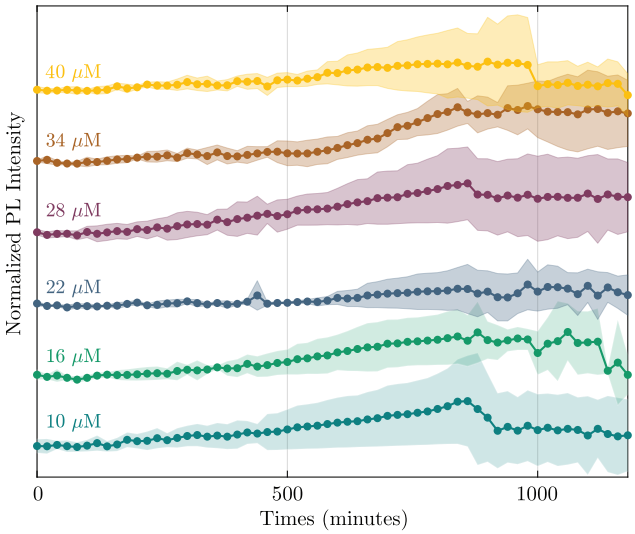

Figure S10: ThT fluorescence intensity as a function of time for PEG-crowded Aβ fibrils treated with varying concentrations of EPPS. Shaded regions indicate the standard deviation of ThT intensity from three independent measurements.

12 FTIR spectrum of PEG-crowded Aβ

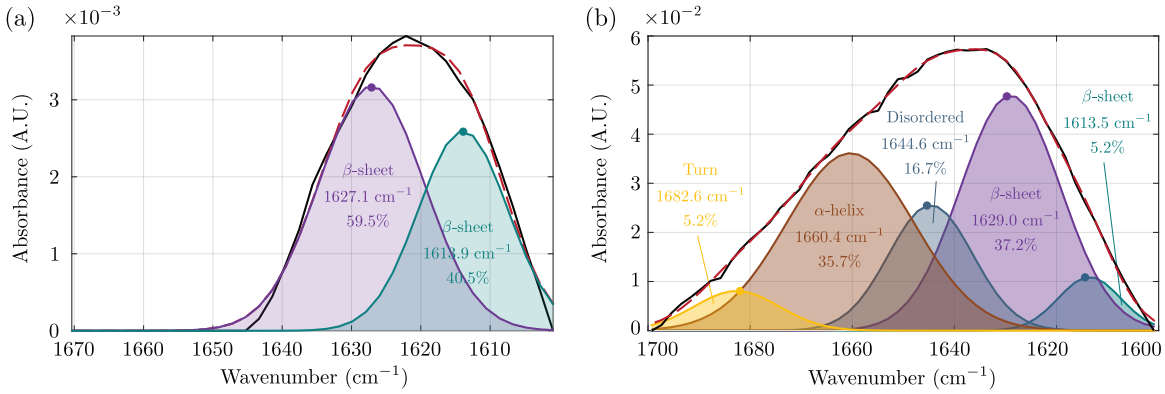

Figure S11: (a) FTIR spectrum of PEG-crowded Aβ fibrils. The amide I region reveals that nearly the entire sample adopts a β-sheet conformation, indicating a highly ordered fibrillar structure under macromolecular crowding conditions. (b) FTIR spectrum of PEG-crowded Aβ fibrils treated with 10 μM EPPS for 4 h. The amide I region reveals a substantial decrease in β-sheet content to approximately 40%, accompanied by the emergence of an α-helical peak as the dominant secondary structure, indicating pronounced structural reorganization upon EPPS treatment under crowded conditions.

13 FTIR analysis of PEG crowded EPPS-treated Aβ during early incubation intervals

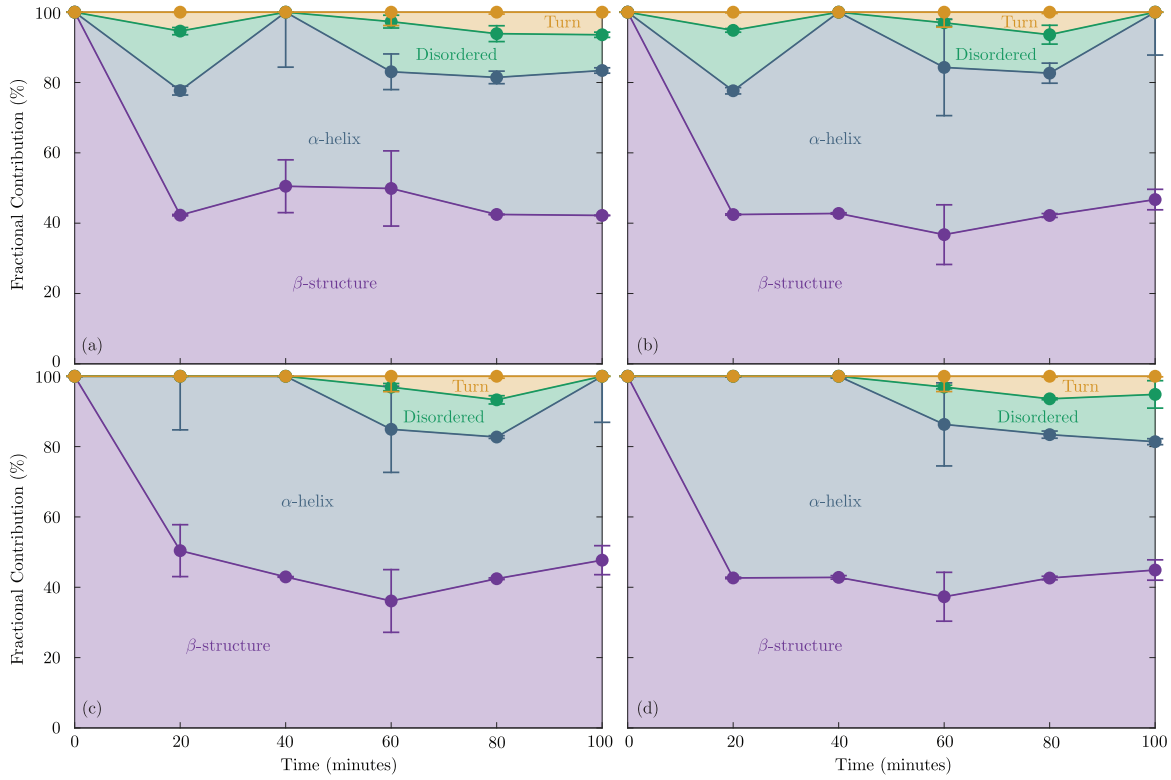

Figure S12: FTIR disaggregation analysis showing concentration-dependent changes in Aβ secondary structures upon treatment with (a) 10 μM , (b) 20 μM, (c) 30 μM and (d) 40 μM EPPS for 100 minutes. Fractional contribution of β and other secondary structures during EPPS treatment are shown as a function of time for the early 100 minute interval.

References

[1] C. F. Bohren and D. R. Huffman, Absorption and Scattering of Light by Small Particles (John Wiley & Sons, Ltd, 1998).